Outstation for X-ray Powder Diffraction at the Italian beamline at the European Synchrotron

G. O. Lepore,[1] S. Checchia,[2] T. Baroni,[3] M. Brunelli,[4] and F. d'Acapito[4]
[1)] *Dipartimento di Scienze della Terra, University of Florence, Italy*
[2)] *ESRF, 71 Av. des Martyrs, 38043 Grenoble, France*
[3)] *Dipartimento di Scienze della Terra, University of Florence, Italy*
[4)] *CNR-IOM OGG c/o ESRF - LISA CRG, 71 Av. des Martyrs, 38043 Grenoble, France*

(*Electronic mail: brunelli@esrf.fr)

(Dated: 21 September 2022)

LISA (*Linea Italiana per la Spettroscopia di Assorbimento X*), Italian beamline for X-ray Absorption Spectroscopy) is the Italian CRG (*Collaborating Research Group*) beamline at the ESRF (*European Synchrotron Radiation Facility*) dedicated to X-ray absorption spectroscopy (XAS)[1]. In this work a methodical test of the LISA beamline in performing diffraction measurements is carried out. Synchrotron X-ray diffraction measurements would complement absorption spectroscopy techniques with the long-range characterization of the material under investigation, whilst XAS provides the short-range element selective information.

I. INTRODUCTION

LISA (*Linea Italiana per la Spettroscopia di Assorbimento X*), the Italian beamline at ESRF (*European Synchrotron Radiation Facility*) synchrotron,[1] is an instrument dedicated to X-ray Absorption Spectroscopy experiments. The design parameters of the X-ray optics, in particular the high monochromaticity ($\Delta E/E = 1.4 \cdot 10^{-4}$ for the Si(111) crystal and ($\Delta E/E = 6 \cdot 10^{-5}$ for the Si(311) crystal) and the low beam divergence at the sample position (1.8 mrad horizontal, 0.1 µrad vertical), make it also a promising instrument for X-Ray Powder Diffraction (XRPD) measurements. GILDA, the Italian CRG (*Collaborating Research Group*) beamline at ESRF between 1994 and 2014[2], already operated an outstation for time resolved XRPD using a Translating Image Plate[3], permitting the analysis of samples with a time resolution of a few minutes. The outstation presented here has been conceived and realized as a flexible, compact apparatus that will enable the users of LISA to carry out long-range structural investigations complementing the local-structure XAS characterization.

II. EXPERIMENTAL

The primary X-ray beam of LISA is generated by a single bend insertion device with a critical energy of 20.6 keV[1]. The white beam is monochromatized by a fixed-exit nitrogen-cooled Double Crystal Monochromator (DCM) consisting of two pairs of flat silicon crystals (respectively cut along the (311) and the (111) planes). The operative angular range is 3.5–51°, allowing an energy range up to 97 keV using the third harmonic of Si(111) crystal. A collimating cylindrical mirror is placed before the DCM, followed by a focusing toroidal mirror after the DCM[1]. The measurements presented in this work were obtained using the Si(311) crystals of the monochromator, in order to achieve the 4.9 to 72 keV energy operational range.

The XRPD instrument consists of a sample stage with vertical translation (z, see Fig. 1), a support for goniometric heads with a horizontal rotation axis (y) and a large area detector. Specimens can be spinning capillaries or flat-plate specimens, both to be measured in transmission geometry. A beam stop with fine vertical and horizontal translation stages is positioned between sample and detector. At present, the distance between sample and detector can be varied in the range 8 to 22 cm, but it can be modified further if necessary. This setup is installed on the bench for experimental chambers in the second experimental hutch (EH2, see[1]) of the beamline, downstream with respect to the XAS measurement chamber. This arrangement permits an easy switch from XAS to XRPD experiments without removing the XAS instrumentation upstream.

The beam is focused on the sample position (about 1.5 m downstream the standard position used for XAS experiments) by slightly adjusting the incidence angle of the toroidal mirror and its meridional radius of curvature. Using the higher region of the useful range of the Pt-coated mirrors for XRPD experiments allows both to operate with a focussed beam and to keep to a minimum the number of setup operations. In the case presented here the monochromator energy scale was calibrated at the Tellurium K-edge (31.813 keV) collecting the absorption edge of a Tellurium sample. Subsequently, the energy was moved to the indicated values for the data collection. The beam at the sample position had an approximate size of 100 µm x 100 µm (measured using a Basler X-ray camera).

Samples. NIST Standard Reference Materials (SRM) CeO_2 (SRM 674b), Cr_2O_3 (SRM 674b), LaB_6 (SRM 660a), ZnO (SRM 674b), Si (640c) powder samples and $Sr_{0.95}Pr_{0.05}TiO_3$ powder sample were loaded into, respectively, a 0.9 mm diameter quartz capillary, 0.7 mm diameter Kapton tube, 0.3 mm diameter glass capillary, 0.8 mm diameter quartz capillary and 0.3 mm diameters quartz capillary, to optimize transmission (see Table I).

Data collection and reduction. X-ray powder diffraction (XRPD) patterns were collected at room temperature at nominal energy of 38 keV, corresponding to $\lambda = 0.3263(2)$ Å for CeO_2 and Cr_2O_3, and at nominal energy of 39 keV, corresponding to $\lambda = 0.3179(2)$ Å for LaB_6, ZnO, Si and

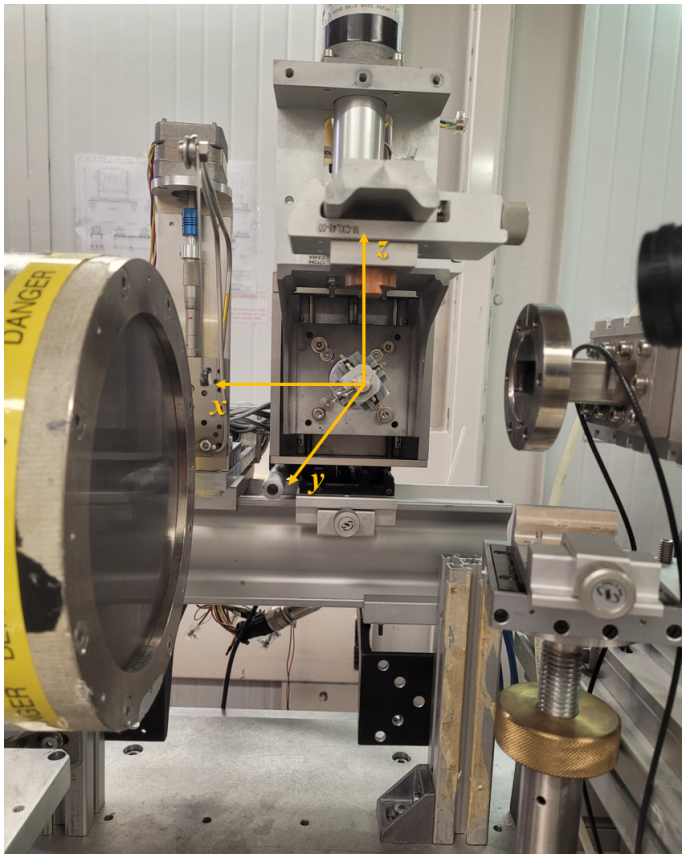

FIG. 1. Photo of the powder diffraction setup at LISA, consisting of a sample stage with vertical translation (z), a support for goniometric heads with a horizontal rotation axis (y) and a large area detector (on the left). X-ray beam travels along the x axis. A beam stop with fine vertical and horizontal translation stages is positioned between sample and detector.

$Sr_{0.95}Pr_{0.05}TiO_3$. A MarResearch (now Rayonix[4]) MAR-165 charge-couple device (CCD) detector was employed for collecting 2-dimensional diffraction images. The detector offers a round sensitive surface area of 165 mm diameter, with 2048 x 2048 pixels in an image in 2 x 2 binning mode, with a resulting pixel size of 80 µm. Samples were aligned for precession and mounted on a goniometer head, spun during the acquisitions in order to improve powder averaging and placed at a sample-to-detector distance of 10.83 cm. 600 seconds total data collection time was employed for CeO_2 and Cr_2O_3 samples, 300 seconds for LaB_6 sample, 90 seconds for ZnO, 150 seconds for Si and 150 seconds for $Sr_{0.95}Pr_{0.05}TiO_3$.

Calibration of the detector geometry was performed using the CeO_2 sample as a reference sample and the pyFAI-calib routine[5,6], giving refined values of detector tilts angle with respect to the incoming beam, sample-to-detector distance, with a fixed value of energy. Azimuthal integration of the 2-dimensional diffraction images was performed using the pyFAI package[5,6]. Figure 2 shows experimental 2-dimensional diffraction images of the six samples.

Data analysis. Experimental XRPD patterns were used for Rietveld refinement of the structural models of the four reference compounds using GSAS-II software package[7]. The background was modelled using N-parameter Chebyshev polynomials; a pseudo-Voigt peak shape was used to model the Bragg reflections; cell parameters were refined starting from NIST certified values, while value of energy/wavelength was kept fix during all cycles of refinements. Agreement factors are reported in Table I.

Analysis of the diffraction data in real space can be performed with the Pair Distribution Function (PDF)[8]. Extraction of the $G(r)$ functions for CeO_2 and Cr_2O_3 samples was performed using PDFGetX3[9] software, employing data for the Fourier Transformation to a Q_{max} = 17.2 Å^{-1}.

III. RESULTS

A. Cell parameters

Figure 3 reports final Rietveld plots for the four reference compounds. In Table I we report refined cell parameters for comparison with NIST certified values. Percentage deviations Δa and Δc are calculated as the percent difference between the refined lattice parameter value and the NIST certified values, which is $\frac{refinedcellparameter-NISTvalue}{NISTvalue} \times 100$. The cell parameters' deviations are thus a measure of the correctness of our experimental method and measurements.

B. Real Space analysis

Figure 4 shows the experimental PDFs of CeO_2 and Cr_2O_3 samples, together with corresponding theoretically calculated PDFs for comparison. A direct analysis of the real space data can be carried out by inspecting the first few interatomic distances. For CeO_2 *Fm-3m* cubic structure, we can observe a first oscillation of the $G(r)$ at about 2.30 Å corresponding to the Ce–O interatomic distance at 2.342 Å, and a second oscillation of the $G(r)$ dominated by the Ce–O distance at 3.8253 Å. For the more complex Cr_2O_3 trigonal *R-32/c* structure, we can observe a first oscillation of the $G(r)$ at about 1.95 Å corresponding to the Cr–O interatomic distance at 1.958 Å, while the O–O interatomic distances at 2.622 Å, 2.737 Å, 2.848 Å, 2.982 Å and the Cr–Cr interatomic distances at 2.673 Å and at 2.886 Å are overlapping with the oscillation present at about 2.84 Å. Relevant oscillations of the $G(r)$ curves are marked with arrows in Figure 4. Broadening of the oscillations of the $G(r)$ limits the resolution in real-space of these PDFs: this is due to the limited experimental Q_{max} and the consequent presence of termination ripples especially at low r. Higher values of exchanged scattering vector Q can be reached by performing diffraction measurement at higher energy and/or employing a larger area X-ray detector.

IV. CONCLUSIONS AND PERSPECTIVE

The results of the tests here described demonstrate the capability of conducting good quality diffraction experiments on

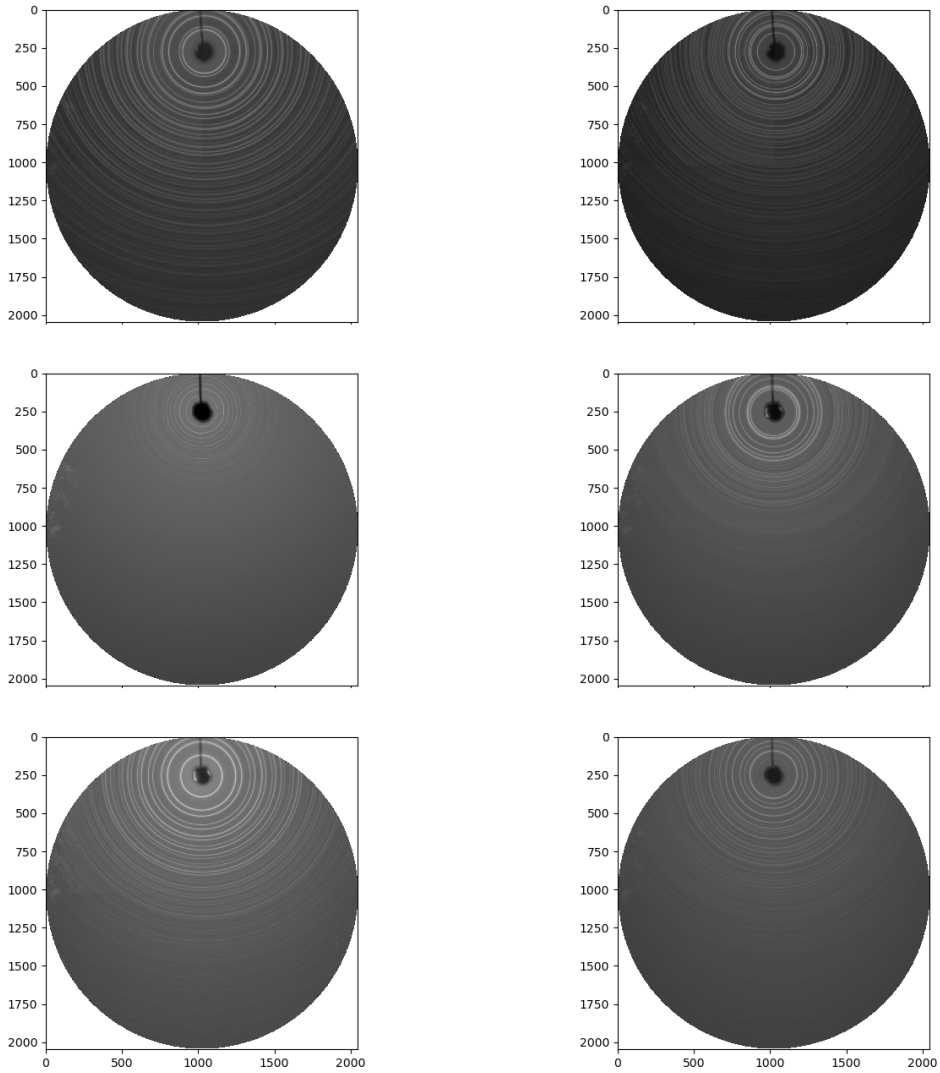

FIG. 2. Experimental two-dimensional (2θ, η) diffraction images of (top left) CeO_2, (top right) Cr_2O_3, (centre left) LaB_6, (centre right) ZnO, (bottom left) Si and (bottom right) $Sr_{0.95}Pr_{0.05}TiO_3$ from LISA beamline at the ESRF (experimental details on data collection strategies in the text and in Table I).

LISA. The comparison of structural parameters obtained on NIST standards shows that the measurements performed with the commissioned XRD setup have good accuracy, thus providing a robust method for phase identification and structural investigations.

Data collection time was not a concern in the static measurements presented in this work, but it can be reduced further, e.g. to one minute per pattern. The detector used for data collection is a MAR-165 CCD, developed and commonly used for standard crystallography performed at 12 keV. At these energies the detector has an efficiency greater than 80%, while at around 38 keV, where this experiment was performed, sensor efficiency drops to about 10%[10], making the counting process inefficient and – as a consequence – slower. The use of cadmium telluride (CdTe, an high-Z semiconductor material) as the sensor material in a 2-dimensional detector would be able to directly convert harder X-ray radiation with excellent absorption power, hence superior detection efficiency at these energies, and much shorter data collection times[11].

The materials of interest to the user community of LISA, both natural and synthetic, are typically amorphous and disordered solids or liquids which often lack long-range order. It is well established that these classes of materials are equally and complementarily well suited investigated using PDF analysis. PDF analysis can give insight about the local structure and its deviation from the average one, even when a limited real space resolution is available[12]. With the current setup, reciprocal space can also be enlarged by tilting the detector. Of course, a larger, high-efficiency single-photon counting 2-dimensional detector designed for high energy X-ray diffraction would al-

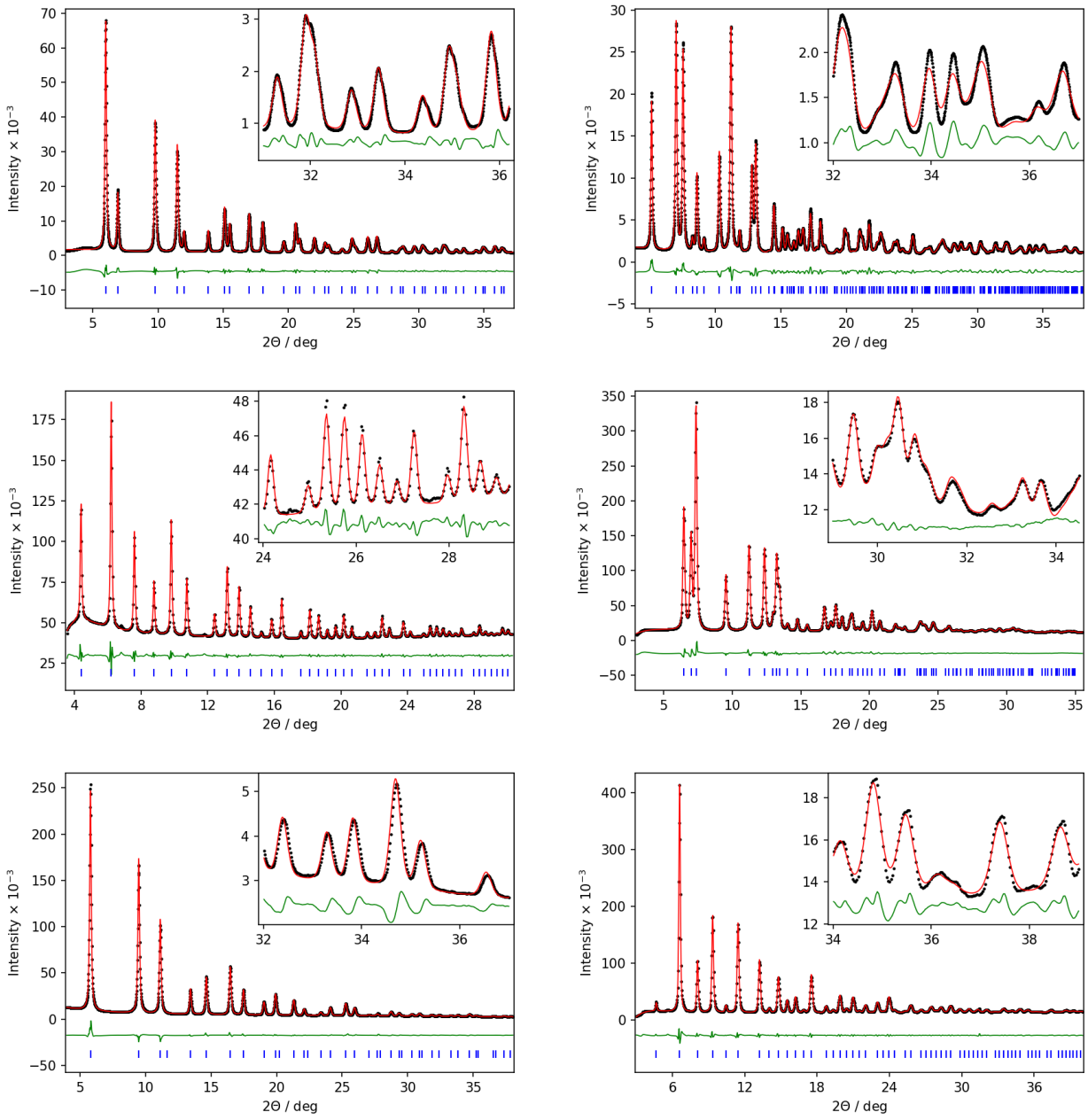

FIG. 3. Observed (black dots), calculated (red line), and difference (offset green line) plots of the final Rietveld refinements of the reference compounds (top left) CeO_2, (top right) Cr_2O_3, (centre left) LaB_6, (centre right) ZnO, (bottom left) Si and (bottom right) $Sr_{0.95}Pr_{0.05}TiO_3$. Reflection positions are shown as vertical line.

low higher values of Q_{max} to be reached so that higher quality $G(r)$ can be extracted in terms of r-resolution, and with shorter measurements. As an example, the Dectris Pilatus3 X CdTe is a widespread choice for a 2-dimensional fast detector, both because of its large active area and the considerations on detector efficiency made above. At the same time, the smaller pixel sizes featured on some of the more compact photon-counting CdTe detectors on the market would not significantly benefit the scientific applications of XRPD experiments at LISA.

Diffraction measurements can be combined with XAS experiments, providing the possibility for users to couple local atomic information with average long-range structural data. In addition, diffraction measurements are a necessary tool for verification of structural changes that might be occurring in the sample after XAS investigation. The XRPD set up is easy-to-install: thanks to its flexible geometry, XRPD measurements can employ standard sample environments: for example, hot air blower for *in-situ* studies as a function of temperature up to 1000°C and a N_2 cryostream down to 80 K. Both systems are currently available to the users of LISA.

TABLE I. Refined cell parameters of reference materials CeO_2, Cr_2O_3, LaB_6, ZnO, Si and comparison with NIST certified values.Δa and Δc are calculated as the percent difference of the refined lattice parameter value with respect to the NIST certified values (formula in the text).

Sample	CeO_2	Cr_2O_3	LaB_6	ZnO	Si
NIST Standard codes	674b	674b	660a	674b	640c
Wavelength / Å	0.3263(2)	0.3263(2)	0.3179(2)	0.3179(2)	0.3179(2)
Capillary	0.9 mm ⌀ quartz capillary	0.7 mm ⌀ Kapton tube	0.3 mm ⌀ quartz capillary	1 mm ⌀ quartz capillary	0.3 mm ⌀ quartz capillary
μR (calculated)[a]	1.8	0.18	0.66	0.73	0.02
Acquisition time / s	600	600	300	90	150
NIST certified lattice parameter, a / Å	5.41153(3)	4.9586(3)	4.1569162(1)	3.24987(1)	5.431195(7)
NIST certified lattice parameter, c / Å	-	13.5965(3)	-	5.20674(1)	-
lattice parameter, a / Å	5.40997(8)	4.9544(2)	4.1607(1)	3.2504(1)	5.43702(8)
lattice parameter, c / Å	-	13.5834(4)	-	5.2085(2)	-
Δa (%)	0.03	0.08	0.09	0.02	0.10
Δc (%)	-	0.09	-	0.03	-
R_{wp}(%)	6.3	4.8	1.3	2.9	3.7
GOF	1.03	0.78	0.96	1.41	2.11

[a] μR is calculated using https://11bm.xray.aps.anl.gov/absorb/absorb.php assuming a packing fraction of 0.5.

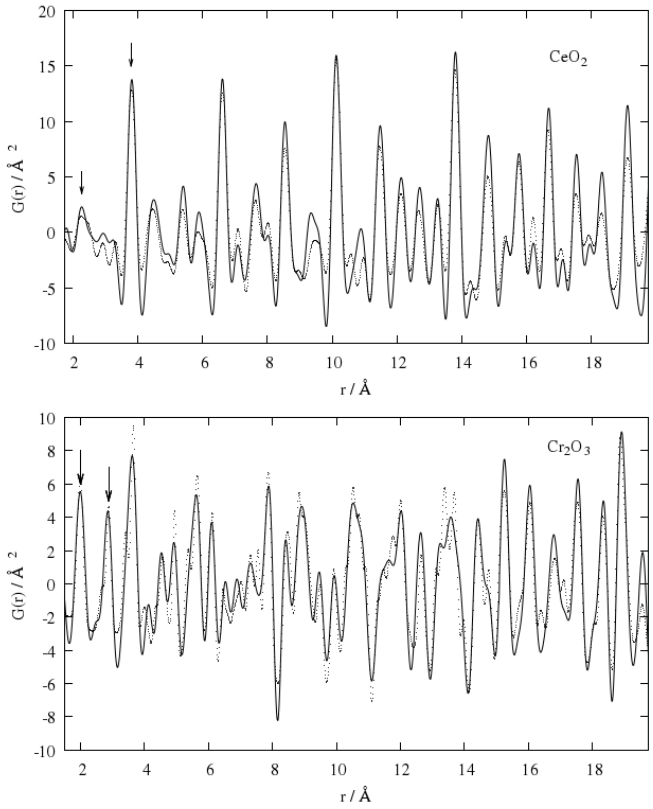

FIG. 4. Experimental (line) and calculated (dotted line) PDFs of CeO_2 (top panel) and Cr_2O_3 (bottom panel) samples from X-ray data collected at BM08/LISA beamline at the ESRF plotted up to r = 20 Å.

The possibility to have both XAS and XRD on the same beamline at the synchrotron is rare. One distinguished example is the BM31 beamline of the Swiss-Norwegian Beamlines at the ESRF[13] where XRD and XAS measurements can be performed quasi-simultaneously thanks to two dedicated monochromator systems that can switch within seconds. The features presented here for LISA highlight the unique possibility to develop a large variety of diffraction experiments coupled with XAS investigations. To quote some instances, the relatively quick measurement times, together with the wide energy range attainable at LISA, may allow carrying out anomalous diffraction measurements[14,15]. In addition, measuring sets of samples or positions within a flat sample would be possible by combining a translation stage for the sample mounting. Moreover, the small beam size could be exploited for the installation of a goniometer for single-crystal diffraction.

AUTHOR'S CONTRIBUTIONS

All authors contributed equally to this work.

ACKNOWLEDGMENTS

The authors would like to thank Fabrizio La Manna for technical support on the beamline. LISA is financed by the Consiglio Nazionale delle Ricerche, project DFM.AD006.072.

DATA AVAILABILITY STATEMENT

Raw data were generated at the ESRF large scale facility. Derived data that support the findings of this study are available from the corresponding author upon reasonable request.

[1] F. d'Acapito, G. O. Lepore, A. Puri, A. Laloni, F. La Manna, E. Dettona, A. De Luisa, and A. Martin, "The LISA beamline at ESRF," Journal of Synchrotron Radiation **26**, 551–558 (2019).

[2] F. d'Acapito, S. Colonna, S. Pascarelli, G. Antonioli, A. Balerna, A. Bazzini, F. Boscherini, F. Campolungo, G. Chini, G. Dalba, I. Davoli, P. Fornasini, R. Graziola, G. Licheri, C. Meneghini, F. Rocca, L. Sangiorgio, V. Sciarra, V. Tullio, and S. Mobilio, "GILDA (Italian Beamline) on BM8," ESRF Newsletter **30**, 42–44 (1998).

[3] C. Meneghini, G. Artioli, A. Balerna, A. F. Gualtieri, P. Norby, and S. Mobilio, "Multipurpose imaging-plate camera for *in situ* powder XRD at the GILDA beamline," Journal of Synchrotron Radiation **8**, 1162–1166 (2001).

[4] www.rayonix.com, .

[5] G. Ashiotis, A. Deschildre, Z. Nawaz, J. P. Wright, D. Karkoulis, F. E. Picca, and J. Kieffer, "The fast azimuthal integration Python library: *pyFAI*," Journal of Applied Crystallography **48**, 510–519 (2015).

[6] J. Kieffer, V. Valls, N. Blanc, and C. Hennig, "New tools for calibrating diffraction setups," Journal of Synchrotron Radiation **27**, 558–566 (2020).

[7] B. H. Toby and R. B. Von Dreele, "*GSAS-II*: the genesis of a modern open-source all purpose crystallography software package," Journal of Applied Crystallography **46**, 544–549 (2013).

[8] S. J. L. Egami, T.; Billinge, *Underneath the Bragg peaks*, Pergamon Materials Series (Pergamon Press, 2003).

[9] P. Juhás, T. Davis, C. L. Farrow, and S. J. L. Billinge, "*PDFgetX3*: a rapid and highly automatable program for processing powder diffraction data into total scattering pair distribution functions," Journal of Applied Crystallography **46**, 560–566 (2013).

[10] J. Jakoncic, M. Di Michiel, Z. Zhong, V. Honkimaki, Y. Jouanneau, and V. Stojanoff, "Anomalous diffraction at ultra-high energy for protein crystallography," Journal of Applied Crystallography **39**, 831–841 (2006).

[11] J. Schultheiß, L. Liu, H. Kungl, M. Weber, L. Kodumudi Venkataraman, S. Checchia, D. Damjanovic, J. E. Daniels, and J. Koruza, "Revealing the sequence of switching mechanisms in polycrystalline ferroelectric/ferroelastic materials," Acta Materialia **157**, 355–363 (2018).

[12] M. Coduri, D. Bozzetti, S. Checchia, M. Brunelli, and M. Scavini, "Local and average structure of yb-doped ceria through synchrotron and neutron pair distribution function," Inorganics **7** (2019), 10.3390/inorganics7080102.

[13] P. M. Abdala, H. Mauroy, and W. van Beek, "A large-area CMOS detector for high-energy synchrotron powder diffraction and total scattering experiments," Journal of Applied Crystallography **47**, 449–457 (2014).

[14] M. Allieta, M. Brunelli, M. Coduri, M. Scavini, and C. Ferrero, "Differential pair distribution function applied to $Ce_{1-x}Gd_xO_{2-x/2}$ system," Zeitschrift für Kristallographie Proceedings **1**, 15 (2011).

[15] C. Meneghini, A. Balerna, F. Boscherini, S. Pascarelli, and S. Mobilio, "Anomalous Wide-Angle X-ray Scattering Apparatus on the GILDA Beamline at the ESRF," Journal of Synchrotron Radiation **5**, 1258–1262 (1998).